The cyclin-G associated kinase (GAK) is a novel mitotic kinase and therapeutic target in diffuse large B-cell lymphoma

Authors: Olivia B. Lightfuss[1], Preet Kumar[2,3], Lingxiao Li[2,3], Toral Shastri[4], Austin D. Newsam[5], Paola Manara[1], Abdessamad Y. Alaoui[2,3], Diego E. Hernandez Parets[13], Pierre A. Younes[13], Dhanvantri Chahar[2,3], Artavazd Arumov[3], Caroline A. Coughlin[5], Indigo P. Williams[6], Nikolai Fattakhov[3], Alicia Bilbao Martinez[7], Ola Landgren[3,8], Stephan C.Schürer[3,9,14], Vance Lemmon[3,10], Francesco Maura[3,8], Daniel Bilbao[3,7], Yangbo Feng[3,9], Hassan Al-Ali[3,10,11,12,14#], Jonathan H. Schatz[2,3#]

[1]Sheila and David Fuente Graduate Program in Cancer Biology; [2]Division of Hematology, Department of Medicine; [3]Sylvester Comprehensive Cancer Center; [4]Internal Medicine Residency Program; [5]Medical Scientist Training Program; [6]Biochemistry and Molecular Biology Graduate Program; [7]Department of Pathology and Laboratory Medicine; [8]Division of Myeloma, Department of Medicine; [9]Department of Molecular and Cellular Pharmacology; [10]The Miami Project to Cure Paralysis, Department of Neurological Surgery; [11]Katz Family Division of Nephrology and Hypertension, Department of Medicine; [12]Peggy and Harold Katz Drug Discovery Center, University of Miami Miller School of Medicine, Miami, FL, USA. [13]University of Miami, Coral Gables, FL, USA; [14]Frost Institute for Data Science &Computing, University of Miami, Coral Gables, FL, USA.
#Corresponding authors:

Jonathan H. Schatz, Division of Hematology, Department of Medicine, University of Miami Miller School of Medicine, 1580 NW 10th Avenue, Batchelor Building, Room # 419, Locator # M877, Miami, FL 33136-1000, E-mail: jschatz@med.miami.edu, Tel: 305-243-7742

Hassan Al-Ali, Department of Neurologic Surgery, University of Miami Miller School of Medicine, , E-mail: halali@med.miami.edu, Tel: 305-243-8491

Running Title: GAK is a novel therapeutic target in DLBCL

Text word count: 3959

Abstract word count: 249

Number of figures: 7

Number of references: 72

Data Sharing Statement: All data in this study were generated by the authors or were analyzed from primary sources cited and are available as needed upon request from the corresponding author. The RNA sequencing data we generated are publicly available from the Gene Expression Omnibus (https://www.ncbi.nlm.nih.gov/geo/, GEO) under accession# GSE279610.

KEY POINTS:

• Phenotypic screening and target deconvolution revealed GAK as a novel therapeutic target in diffuse large B-cell lymphoma

• GAK kinase activity is a key requirement for successful mitosis in DLBCL linked to deficiency of the retinoblastoma (RB) tumor supressor

Abstract: Diffuse large B cell lymphoma (DLBCL) is an aggressive non-Hodgkin lymphoma and the most frequently diagnosed hematologic malignancy in the United States. DLBCL exhibits significant molecular and clinical heterogeneity, and at least a third of patients are left uncured with standard frontline chemoimmunotherapy. As such, there is a critical need to identify novel targeted therapies to improve outcomes. We conducted a phenotypic screen of kinase inhibitors against DLBCL cell lines and non-malignant controls. We identified the cyclin G-associated kinase (GAK) as a tumor-selective, readily druggable target whose inhibition killed DLBCL cell lines, while sparing non-malignant blood cells. Upon investigation of GAK's cellular function, we discovered that inhibition results in G2/M-phase cell cycle arrest. Immunofluorescent confocal microscopy revealed significant chromosome misalignment and spindle distortion in DLBCL cells following GAK-inhibition, disrupting progression through mitosis. Analysis of RNA-seq data from clinical samples showed increased *GAK* expression associates strongly with *RB1* deficiency in DLBCL cases, suggesting dependency on GAK for proper mitotic progression linked to retinoblastoma associated protein (RB) loss of function, a common DLBCL driver. In cell-cycle analyses and under microscopy, RB-deficient DLBCL cells treated with an exquisitely selective GAK inhibitor showed complete arrest at G2/M, pronounced distortion of mitotic spindles, and widespread chromosomal damage. Finally, in vivo studies of DLBCL xenograft-bearing NSG mice achieved a dramatic tumor-burden reduction in response to targeted GAK inhibition. These results reveal a novel cell cycle kinase suitable for therapeutic exploitation in DLBCL patients and linked to the common, undruggable biomarker of RB loss of function.

Introduction: Diffuse large B-cell lymphoma (DLBCL) is among the most frequently diagnosed hematologic malignancies, comprising a clinically and molecularly heterogeneous group of sub-entities.[1,2] Gene-expression profiling two decades ago divided DLBCL into germinal center B-cell (GCB) and activated B-cell (ABC) cell-of-origin (COO) subtypes, with the latter carrying worse prognosis.[3,4] Subsequent genomics studies defined 5-7 molecular subgroups based on varying frequency of recurrent alterations.[3,5–7] Despite greatly increased comprehension of disease biology, however, there has been little progress developing interventions directed at specific subtypes. R-CHOP (rituximab, cyclophosphamide, doxorubicin, vincristine, and prednisone) chemoimmunotherapy remains standard frontline treatment regardless of molecular characteristics.[8–11] A recent substitution of vincristine with the anti-CD79B antibody-drug conjugate polatuzumab vedotin (pola-R-CHP) introduces a new alternative with improved progression-free survival, but frontline treatment choices remain largely uninformed by the prognostic significance of molecular biomarkers, and at least 30-40% of patients will not achieve cure.[12–15] CD19-directed chimeric antigen receptor T-cells (CAR-19) are potentially curative new salvage options.[16–18] These resource-intensive therapies are only available at selected specialized centers, however, and a third or less of patients achieve cure from the approach.[19–21]

Targeted therapies such as Bruton's tyrosine kinase (BTK) inhibitors have revolutionized care of other B-lymphomas but strikingly have found little role in the management of DLBCL.[22–26] ViPOR (venetoclax, ibrutinib, prednisone, obitutuxumab, lenalidomide) showed promising response rates in heavily pretreated patients and is the first successful DLBCL regimen with a kinase inhibitor as well as the first to exclude traditional chemotherapy agents completely,[26] but long-term followup for better assessment of response duration is pending. As things stand, salvage chemoimmunotherapy, requiring stem cell transplant consolidation in second-line settings, and CAR-T cells remain the only potentially curative treatment paradigms for relapsed or refractory (rel/ref) DLBCL, most of whom unfortunately will die from complications of disease progression.[27,28]

Utilizing a first-of-its kind phenotypic screen of kinase inhibitors against DLBCL cell lines, we identified the cyclin G-associated kinase (GAK) as a novel, cancer-selective target in both GCB and ABC DLBCL. GAK is characterized as a participant in clathrin-mediated endocytosis and vesicular trafficking, but we instead find critical roles for its kinase function in successful cell-cycle progression.[29–32] This study is the first to characterize GAK as a therapeutic target in DLBCL or other malignancy. Critically, we overcame barriers to in vivo evaluation of GAK inhibition to establish therapeutic window and therefore proof-of-principle for GAK as a novel therapeutic target.

Methods

Cell Lines, Reagents, Viability Studies

Cell were maintained in culture media according to supplier guidelines. Sources of compounds in cell-based experiments are in **Table S1**. To determine drug viability effects, cells were seeded in 96-well plates at 3,000-5,000/well in serial 1:2 dilutions for 72 hours and assessed by CellTiter-Glo (Promega). For synergy assays, cells were incubated with drug combinations for 72 hours. Viability data were analyzed using the SynergyFinder tool to calculate Bliss Synergy Score.

Phenotypic Screen
The Published Kinase Inhibitor Set (PKIS-I) library was screened as previously described.[33,34] Differential drug sensitivity scroring (dDSS) was calculated using the DSSR software package.[35]

Target Deconvolution Analysis
Target deconvolution was as previously described.[33] Kinase activity profiles were from previously published data.[36] Target deconvolution was performed using previously described computational methods.[33,34,37]

siRNA Validation
Dharmacon Acell siRNAs from Horizon were introduced followed by viability assessment by CellTiter-Glo (Promega). For initial validation, siRNA effects were calculated as robust and differential z-scores compared to PBMCs **(Table S3)**.

Growth Inhibition
Cells were seeded in 96-well plates at 3,000-5,000/well and treated as indicated. After 48 hours, treatment was refreshed. Growth inhibition was assessed at 96 hours by CellTiter-Glo (Promega).

Western Blot
Cells were lysed and protein quantified using Bradford reagent (Biorad). Proteins were resolved on SDS-PAGE and transferred to PVDF membranes (Biorad) according to manufacturer protocol. Membranes were probed with primary and secondary antibodies **(Table S2)** with chemiluminescence measured by LiCor imaging.

RNA Sequencing
U2932 and Ly1 cells were treated in triplicate with vehicle (DMSO) or 1 µM SGC-GAK-1 for 12 and 24 hours. RNA was extracted using the Qiagen Symphony and quantified with Qubit. Libraries were sequenced on the Illumina Novaseq X platform. Samples were polyA selected and generated approximately 30 million PE150 reads/sample. Differential expression was determined using edgeR and limma at log-2 fold change > 0.5, adjusted p-value < 0.05 cutoffs. Gene-set enrichment analysis (GSEA) employed FGSEA, with a false discovery rate (FDR) q value threshold <0.25.

Flow Cytometry Cell Cycle Analysis
Cells were stained with Vybrant™ DyeCycle™ Orange Stain (Thermo Fisher) according to the manufacturer's protocol and read using a flow cytometer at 488 nm and analyzed in FlowJo software.

Immunofluorescent Confocal Imaging
Adherent cells were seeded on glass coverslips in 12-well plates. Suspension cells were seeded in 6-well plates. Cells were treated with SGC-GAK-1 or vehicle, fixed with 4% paraformaldehyde, blocked with blocking buffer (Cell Signaling), stained with primary antibody (anti-alpha tubulin, Thermo Fisher), secondary antibody (Goat anti-Mouse Alexa Fluor™ 488, Thermo Fisher), and DAPI (Thermo Fisher). Imaging was on a Leica confocal microscope.

NanoBRET® Target Engagement (TE) Intracellular Kinase Assay
The NanoBRET® TE Intracellular Kinase Assay kit (Promega, #N2640) and NanoLuc®-GAK Fusion Vector (Promega, NV142A) were used according to manufacturer protocol in 293T cells during compound exposures with BRET ratios calculated in GraphPad Prism.

***In vivo* Experiments**
All mouse studies were approved by the University of Miami Institutional Animal Care and Use committee. Luciferase-engineered U2932 cells (1 × 10^6) were injected intravenously by tail vein, and treatment began one day later. Mice in the ABT + SGC-GAK-1 group received 50 mg/kg 1-aminobenzotriazole (ABT) 2 hours before 10 mg/kg of SGC-GAK-1, both by oral gavage. Vehicle-treated mice received 10% DMSO, 40% PEG 300, 5% Tween 80, and 45% saline. Treatments were administered daily.

Immunohistochemistry
Tissues were fixed in 10% formalin. All the staining used a Bond RX automated stainer (Leica Microsystems) and visualized using a Leica microsystem (CMS GmbH).

Quantification and Statistical Analysis
Experiments were performed in three independent replicates unless otherwise noted. Statistical analyses employed GraphPad Prism version 9. Unpaired student's t test and ANOVA statistical significance: ns, $p > 0.05$; *$p \leq 0.05$; **$p \leq 0.01$; ***$p \leq 0.001$ and ****$p \leq 0.0001$).

For detailed description of the methods, please refer to the supplemental Materials, available on the Blood website.

Results:

Phenotypic Screening Identifies GAK as a Novel Drug Target Candidate in DLBCL

To identify drug targets that sensitize DLBCL across subtypes, we conducted a phenotypic screen of kinase inhibitors against 6 GCB- and 4 ABC-derived cell lines with peripheral blood mononuclear cells (PBMCs) as non-malignant control **(Fig. 1A)**.[38] For each inhibitor, we calculated a Drug Sensitivity Score (DSS) and differential DSS (dDSS), subtracting the DSS for each inhibitor with PBMCs from the inhibitor's DSS of each cell line **(Fig. 1B, Table S4)**.[35] As such, the dDSS scores each inhibitor on cancer-vs-normal selective efficacy with dDSS ≥10 considered initial hits. We next performed target deconvolution using idTRAX to further reveal those kinases most strongly driving cancer-selective effects **(Table S5)**.[33,34,37,39] Established drug targets aurora kinase A (AURKA) and the delta isoform of phosphinositide 3-kinase (PI3Kδ) were hits, while the cyclin-G associated kinase (GAK) emerged as a novel target. The Aurora kinases have been explored as therapeutic targets in cancer due to critical roles regulating multiple steps of the cell cycle but faced clinical challenges due to poor efficacy within acceptable limits of toxicity.[40,41] Phase I evaluation in DLBCL found responses including complete responses limited to non-GCB cases, but high rates of grade 3+ hematologic toxicities discouraged further development.[42] PIK3δ is the target of idelalisib, which was approved to treat

relapsed indolent lymphomas but came off the market in 2022 due to high rates of hepatotoxicity.[43] We therefore focused on GAK, an understudied kinase and novel target in cancer therapeutics.

To validate idTRAX results, we assessed siRNA knockdown of the top 10% of hits in two GCB and two ABC cell lines, confirming PI3Kδ, AURKA and GAK **(Fig. 1C, Table S3)**. We then performed a second siRNA confirmation with GAK, PI3Kδ (positive control), PTK2B (negative screen hit), and a non-targeting control (siNT, **Fig. 1D)**. Si*GAK* consistently promoted decreased viability, but we wanted to validate importance of GAK's kinase function. We therefore employed the exquisitely selective GAK inhibitor SGC-GAK-1, alongside its GAK-sparing analog SGC-GAK-1N **(Fig. 1E)**.[44] Since anti-GAK activity is the only difference between SGC-GAK-1 and SGC-GAK-1N, results strongly validated that GAK kinase activity inhibition is a DLBCL vulnerability. Through phenotypic screening, followed by validation with RNAi and chemical inhibition, we identified GAK as a candidate drug target in DLBCL.

GAK Inhibition is Broadly Active against DLBCL Without Impact on B-Cell Receptor Signaling or Recycling

We therefore undertook broader assessment of GAK inhibition, assessing growth inhibition with SGC-GAK-1 on a large panel of DLBCL lines **(Fig. 2A)**. The compound showed ≤1 μM GI_{50} across these systems. ABC-derived ines were significantly more sensitive than those derived from GCB cases (p=0.0078) **(Fig. 2B)**. Various other hematologic and solid-tumor malignancies also demonstrated sensitivity **(Fig. S1)**. GAK is a clathrin heavy chain (CHC) binding partner and component of clathrin-coated vesicles during endocytosis, whose disruption can alter oncogenic signals.[31,45–49] B-cell receptor (BCR) signaling drives DLBCL pathogenesis and employs trafficking to recycle BCR components to the cell surface after activation-induced endocytosis and to form MYD88-TLR9- BCR (My-T-BCR) supercomplexes in endolysosomes.[50,51] This compelled us to assess whether GAK inhibition would impact these processes. GAK inhibition had no apparent impact on BCR-activated signaling pathways, demonstrated by sustained phospho- and total AKT and ERK levels following SGC-GAK-1 treatment **(Fig. 2C).** There also was no reduction BCR cell-surface expression upon SGC-GAK-1 treatment, indicating no impact on BCR recycling **(Fig. 2D)**. Broad anti-lymphoma activity of highly selective GAK kinase inhibition therefore does not appear clearly related to the target's roles in endocytosis or vesicular trafficking.

GAK Inhibition Triggers Induction of the Mitotic Spindle Assembly Checkpoint and G2/M-Phase Cell-Cycle Arrest

Previous studies implicated GAK in centrosome integrity and alignment of mitotic spindles during M phase.[30,32] Specifically, GAK siRNA knockdown caused spindle-assembly checkpoint (SAC) activation and metaphase arrest, characterized by misaligned and abnormally condensed chromosomes.[30] Subsequently, Wolf et al. found GAK knockdown disrupted spindle positioning, notably of astral microtubules.[32] The role, if any, of GAK's kinase function in these effects was undefined, however.[32] We therefore assessed mitotic impact of SGC-GAK-1 in DLBCL. Strikingly, western blotting across lines demonstrated robust SAC activation following SGC-GAK-1 treatment indicated by phosphorylation of Histone 3 (pH3) and variable increases of total H3, Cyclin B1, and BUB1B **(Fig. 3A)**.[52–55] Cell cycle assessment by quantitative DNA

flow cytometry revealed accumulation at G2/M 24 hr following SGC-GAK-1 treatment that was more pronounced than the positive control flavopiridol, a multi-kinase inhibitor known to induce G2/M arrest **(Fig. 3B)**.[56] These results suggest GAK kinase activity is crucial for proper mitosis, aligning with its previously described, though poorly characterized, role in regulating mitotic spindles.[30,32] Further supporting these observations, immunofluorescent confocal imaging revealed pronounced distortion of spindles and misalignment of chromosomes in response to SGC-GAK-1 compared to vehicle **(Fig. 3C)**. Immunofluorescence quantification of DAPI-stained chromosomes confirmed significant arrest at G2/M, while PBMCs were spared **(Fig. 3D)**. Therefore, in cultured cells, effects on mitosis predominated over any role for GAK in vesicular trafficking related to BCR signaling, implicating GAK as a potentially critical and novel cell-cycle kinase in DLBCL.

GAK Expression Associates with Cell Cycle Activation in DLBCL Cases

To assess clinical relevance of these findings, we analyzed DLBCL gene-expression profiling (GEP) datasets. We divided cases from the Reddy dataset (n=775 with RNA-seq) into four quartiles based on *GAK* expression.[57] Comparing *GAK*-high (Q4) to *GAK*-low (Q1) cases, we found 1,501 differentially expressed genes at adjusted $p<0.05$, log-2 fold change >0.5. Gene-set enrichment analysis by FGSEA[58] revealed 34 gene sets upregulated in Q4 vs. Q1 at a strict false discovery rate $q<0.05$. Strikingly, 11/34 were directly relevant to GAK's known roles in biology, mitosis, and vesicular trafficking **(Fig. 4A)**. For validation, we explored 75 DLBCL cases in the Pan-Cancer Analysis of Whole Genomes (PCAWG) data with available RNA-seq.[59] Despite the relatively lower power of the smaller dataset, there were 599 differentially expressed genes between *GAK* Q4 and Q1. FGSEA strongly validated convergence on mitosis and trafficking functions in 13/60 gene sets at $q<0.05$ **(Fig. 4A)**. Both datasets implicate MITOTIC_SPINDLE_ASSEMBLY as strongly activated in *GAK*-high cases (red arrows). These data implicate GAK as a key participant in cell-cycle progression in DLBCL tumors, consistent with our cell-line findings.

Previous studies of acute cell-cycle disruption by AURKA inhibitor alisertib showed down-regulation of cell-cycle factors at the level of mRNA expression as part of the overall cellular response.[60] We therefore performed bulk RNA-seq on U2932 (ABC) and Ly1 (GCB) cells treated in triplicate with 1 µM SGC-GAK-1 or DMSO for 12 and 24 hours. Unsupervised clustering showed clear separation between SGC-GAK-1 and DMSO conditions **(Fig. S2)**. In U2932 cells, 85 and 412 genes were differentially expressed at 12 and 24 hours, respectively ($p < 0.05$, log-2 fold change > 0.5). Similarly, 100 and 749 genes were differentially expressed in Ly1. FGSEA revealed upregulation of Hallmark pathways governing cell-cycle progression, including E2F_TARGETS, G2M_CHECKPOINT, and MITOTIC_SPINDLE, in both lines at both time points **(Fig. 4B)**. Gene ontology (GO) pathways were highly consistent **(Fig. S3)**. These results suggest cellular responses that activate proliferative gene-expression programs to overcome SAC induction following GAK inhibition, including MYC_TARGETS and MTORC1_SIGNALING **(Fig. 4B)**.[61,62] Notably, nearly all of the top 20 significantly upregulated GO pathways were linked to cell cycle progression **(Fig. S3)**. We note that SAC induction in DLBCL occurred in response to SGC-GAK-1 but not alisertib **(Fig. 4C)**. Together, these results support the essential role of GAK kinase function in maintaining proper cell cycle control in ABC and GCB DLBCL. Disrupted cell cycle in GAK-inhibited cells triggers compensatory transcriptional responses and upregulation of cell-cycle related pathways, in marked contrast to

observations for alisertib.[60]

Based on the observed enrichment of mitotic gene expression in response to the block at G2/M, we investigated potential for synergistic interactions between SGC-GAK-1 and other drugs with antimitotic activities. We tested SGC-GAK-1 combined with DLBCL chemotherapeutics and various targeted cell-cycle inhibitors. We assessed 72-hour cell viability effects by SynergyFinder Bliss Synergy Score, indicating synergy at >10, additivity ≤10 to -10, or antagonism <-10. Strikingly, the combination treatments consistently showed frequent antagonism across combination approaches and cell lines, and synergy was absent in all **(Fig. 4D)**. These findings suggest GAK inhibition alone profoundly disrupts essential cell cycle processes, rendering additional inhibitors redundant.

GAK Dependence is Strongly Linked to Retinoblastoma Loss of Function in DLBCL

We next examined the broader context of cell-cycle deregulation in disease pathogenesis and how GAK fits into this framework. Cell cycle activation is well-described in B-lymphoma pathogenesis, converging on inactivation of the tumor-suppressive master cell-cycle regulator retinoblastoma associated protein (RB) encoded by *RB1*.[5,63] Research in lung and breast cancers identified the mitotic kinases AURKA and AURKB as critical dependencies in RB-deficient tumors.[64,65] More recently, however, genome-wide CRISPR screening revealed GAK loss-of-function as a synthetic lethal vulnerability in systems with *RB1* deletion, while neither AURKA nor AURKB were hits by this approach.[66] This prompted us to investigate the relationship between *GAK* and *RB1* in the Reddy RNA-seq data and the older chip-based Lenz DLBCL data (n=414).[4,67] The Lenz cohort was divided into high (n=182) and low (n=232) *GAK* groups, while for Reddy with the more quantitative RNA-seq data, we again compared *GAK* Q4 to Q1. Analysis of both datasets show dramatic association between increased *GAK* and reduced *RB1* **(Fig. 5A-B**; p=2.13e-22 and 2.2e-16 respectively**)**. This relationship suggests RB loss-of-function could be a biomarker for potency of GAK inhibition in DLBCL tumors.

We found RIVA and U2932 cells completely lack RB protein **(Fig. 5C)**, and we noted that these lines had by far the most striking arrest at G2/M and mitotic atypia in our initial work with SGC-GAK-1 **(Fig. 3B-C)**. We therefore further assessed these cells compared to RB-competent SU-DHL-4 cells using SGC-GAK-1 and SGC-GAK-1N, both at 1 µM. Flow cytometry showed pronounced G2/M arrest in RIVA and U2932 compared to DHL4 **(Fig. 5D)**, while the GAK-sparing 1N analog had no impact, again highlighting specificity of GAK kinase inhibition as driving these effects. For validation, we wanted to compare systems that were otherwise isogenic, but neither RIVA nor U2932 tolerated *RB1* re-expression, and CRISPR deletion from other lines also proved challenging (not shown). Instead, we employed U2OS human osteosarcoma cells commonly used in cell cycle studies and for which *RB1*-/- CRISPR-modified lines previously were generated and characterized in detail **(Fig. 5E)**.[68] Growth inhibition assays showed the *RB1*-/- clone was significantly more sensitive to SGC-GAK-1 than wild-type **(Fig. 5F**, GI_{80} 0.651 and 3.494 µM respectively**)**. By confocal imaging, untreated RB-deficient U2OS had chromosomal abnormalities compared to WT as previously reported **(Fig. 5G**, DMSO-treated**)** and were especially sensitive to SGC-GAK-1 with profound chromosomal and mitotic-spindle atypia and accumulation at G2/M **(Fig. 5G-H)**. Our findings demonstrate tumors with cell-cycle deregulation due to RB-deficiency are particularly sensitive to GAK inhibition, with significant effects on cell-cycle progression and mitotic integrity.

Efficacy of GAK Inhibition In Vivo

SGC-GAK-1 is a tool compound with exquisite selectivity for GAK.[44] While it's an ideal chemical probe *in vitro*, the compound is challenging for *in vivo* investigation. This is due to high metabolic susceptibility to P450 enzymes (mouse liver microsomes $t_{1/2}$ 5.7 min), which results in first-pass hepatic metabolism and a poor in vivo PK profile ($t_{1/2}$ <1 hr, C_{max} <100 ng/mL).[69] However, SGC-GAK-1 can be used in vivo when combined with a 2-hr pretreatment of 50 mg/kg 1-aminobenzotriazole (ABT), a broad spectrum cytochrome P450 inhibitor to extend half life ($t_{1/2}$ ~3 hr, C_{max} 650 ng/mL).[69] Importantly, ABT treatment has no effect on DLBCL cell lines and does not exhibit toxicity towards non-malignant PBMCs **(Fig. S4)**. We tail vein injected 10^6 luciferase-engineered U2932 cells into NSG mice and treated with vehicle or SGC-GAK-1 (10mg/kg) with ABT pretreatment. SGC-GAK-1 achieved significant tumor burden reduction compared to the vehicle (p=0.0003) **(Fig. 6A-B)**. Immunohistochemistry (IHC) of lung and liver tissue samples showed marked decrease in the Ki67 proliferation marker in SGC-GAK-1 treated samples **(Fig. 6C)**.

Despite the substantial reduction in TV, the difference in OS was less **(Fig. 6D)**. This discrepancy can be attributed to the poor pharmacokinetics of SGC-GAK-1, resulting in incomplete systemic distribution across organs **(Fig. 6E)**. Even with ABT co-administration, SGC-GAK-1 $t_{1/2}$ is only ~3 hours. Ex vivo IVIS signal in individual organs revealed significant reduction in tumor burden in lungs, liver, and spinal cord of SGC-GAK-1 treated mice. However, no significant differences were observed in femur, brain, or spleen, indicating poor distribution of intact SGC-GAK-1 to these organs **(Fig. 6E)**. While this limitation likely impacted the ability to fully eradicate disseminated disease, our results indicate that GAK can be effectively targeted in vivo to reduce tumor burden without associated toxicities. Development of GAK inhibitors with improved pharmacokinetic profiles is essential to enhance therapeutic outcomes and permit translation to patients over the longer term.

Candidate Clinical Drugs for GAK Repurposing

To expedite clinical translation, drug repurposing offers a promising approach. In addition, it permits orthogonal target validation through use of additional compounds that inhibit GAK's kinase activity, of which there are few others besides SGC-GAK-1 reported. We explored available kinome profiling data reported for kinase inhibitors developed for clinical use and found GAK is a potential off-target of several clinically available compounds, including several FDA-approved drugs.[70] Repurposing these existing compounds can leverage established pharmacokinetics, dosing, and safety profiles to GAK as a novel target. Strikingly, several compounds are reported to have significantly higher binding affinity for GAK compared to their intended clinical target, as indicated by their lower Kd values from published biochemical assays **(Fig. 7A)**.[71] We obtained these compounds and performed NanoBRET live-cell target engagement assays to assess their intracellular binding to GAK. The intracellular Kd for OTS167, milciclib, bosutinib, gilteritinib, and fedratinib demonstrated stronger GAK affinity than SGC-GAK-1 **(Fig. 7B)**. We next assessed selected compounds' potency against DLBCL cell lines by growth inhibition assays. Milciclib GI_{50} ranged from 0.2 to 0.3 uM across GCB and ABC DLBCL cell lines **(Fig. 7C)**. OTS167, whose GAK NanoBRET IC_{50} was more than two orders of magnitude more potent than SGC-GAK-1 at 1.4 nM, demonstrated GI_{50} <10nM across

multiple lines **(Fig. 7D)**. Both OTS167 and milciclib were found to activate the SAC, with G2/M cell cycle arrest demonstrated also by flow cytometry **(Fig. 7E-F)**. Notably, the most pronounced effects were observed with OTS167 at 1 nM. This is likely due to the compound effectively inhibiting GAK at this lower concentration, while minimizing off-target effects. At higher concentrations, inhibition of additional kinase targets likely leads to additional consequences that overshadow the specific impact on GAK's role in cell-cycle regulation. These findings provide orthogonal GAK target validation and highlight the potential for rapid clinical translation by repurposing existing kinase inhibitors against GAK.

Discussion: DLBCL is characterized by significant molecular and clinical heterogeneity, yet current treatments rely predominantly on standard chemoimmunotherapy, which fails to cure more than a third of patients.[1–3,5,7–11] This highlights urgent need for novel, targeted therapies to improve patient outcomes. Our study addresses this by identifying GAK as a promising therapeutic target in DLBCL through a comprehensive phenotypic screen of kinase inhibitors. GAK is a CHC binding partner and participant in endocytosis and vesicular trafficking. Previous studies showed that, like CHC, GAK localizes to mitotic spindles, and its siRNA knockdown promoted spindle positioning defects, multi-aster formation, and chromosomal defects in post-mitotic cells.[29–32] The role if any of its S/T kinase activities in cell cycle regulation, however, remained unclear. We reveal that GAK kinase inhibition exhibits tumor-selective potency against DLBCL, sparing nonmalignant cells. Through flow cytometry, western blotting, and immunofluorescent microscopy, we demonstrate that GAK inhibition disrupts mitosis by causing chromosome misalignment and spindle distortion, leading to SAC activation and cell cycle arrest. These findings therefore establish for the first time that GAK is a cell cycle kinase whose inhibition results in anti-tumor activity.

Analyses of clinical datasets reveal higher *GAK* expression strongly associates with pathways involved in mitotic spindle assembly. RNA-seq intriguingly showed consistent up-regulation of genes associated with the mitotic spindle, G2/M arrest, and cell-cycle progression in GAK inhibitor-treated cells. These findings stand in contrast to alisertib, the clinical inhibitor of AURKA, which has critical roles at multiple phases of the cell cycle.[49,60] GAK kinase activity therefore appears to play narrower, more focal roles, which could provide wider therapeutic windows for its inhibition in cancer treatment compared to AURKA. Alistertib has failed to achieve regulatory approval despite multiple cancer clinical trials, plagued by off-tumor, on-target toxicities.[42,72]

The tumor selectivity of GAK inhibition we observed in vitro translated in vivo with xenografted DLBCL cells showing pronounced sensitivity in mice that experienced no overt toxicities. This occurred despite severe pharmacokinetic limitations of SGC-GAK-1 that required co-administration of the CYP450 inhibitor ABT and even so has a $T_{1/2}$ of only about 3 hours.[69] These results have prompted us to undertake a medicinal chemistry campaign to develop GAK inhibitors with improved properties.

As biomarker, our data reveal specific vulnerability in *RB1*-deficient systems, where GAK inhibition leads to particularly pronounced G2/M arrest. RB loss of function is a common feature of DLBCL cases, and our results therefore promote specific new strategies to target these tumors under a precision-medicine paradigm and potentially independent of other molecular characteristics.[5,63]

Overall, our research defines GAK as a novel and targetable dependency in DLBCL and opens new avenues for targeted therapy development. The frequent off-target inhibition of GAK by clinical kinase inhibitors including several approved drugs further supports feasibility and safety of inhibiting GAK as a therapeutic strategy.[70] Future studies will continue to explore the molecular mechanisms underlying GAK's role in DLBCL pathogenesis, in particular the specific phospho-substrates by which it regulates mitosis, and elucidating the broader impact of GAK inhibition on cancer biology. These efforts will deepen our understanding of DLBCL and contribute to the development of more effective, targeted therapies for this aggressive malignancy.

Acknowledgements: This work was supported by grants from the NIH (1R41TR002293) to H.A., Florida Department of Health (22B13) to J.H.S, H.A, Y.F., and S.S., and a Glaser Foundation Research Award (University of Miami) to H.A. Some experiments occurred at the University of Miami High Content Screening (HCS) Core Facility (RRID:SCR_022542) and the Cancer Modeling and Onco-Genomic Shared Resources (CMSR RRID: SCR022891, OGSR RRID: SCR022502) of the Sylvester Comprehensive Cancer Center at the University of Miami, which is supported by the National Cancer Institute (NCI) of the National Institutes of Health (NIH) under award number P30CA240139. The content is solely the responsibility of the authors and does not necessarily represent the official views of the NIH.

Authorship Contributions: Contribution: O.B.L., P.K., L.L., A.D.N., P.M., D.H.P., P.Y., D.C., A.A., C.A.C., and I.P.W. performed bench experiments. T.S., A.Y.A., O.L., and F.M. oversaw analysis of newly generationed and published gene-expression data. N.F., A.D.M., and D.B. helped design and carry out in vivo experiments. S.C.S. and Y.F. helped design and analyze assessments of compound engagements with GAK. V.L. helped design and supervise phenotypic drug screening. J.H.S. and H.A. supervised all experiments. O.B.L., H.A., and J.H.S. wrote and edited the manuscript with input from all authors, and all authors have approved the final version of the manuscript. H.A. and J.H.S. supervised the project and are responsible for all content.

Disclosure of Conflicts of Interest: The authors declare no relevant competing interests.

Figure Legends:

Figure 1: Phenotypic screen reveals GAK as a novel target for DLBCL
1A: Altered genes in 10 DLBCL lines in the screen, selected to capture genomic diversity.
1B: Differential drug sensitivity (dDSS) scoring of each PKIS-I library compound against each cell line. Formula: dDSS = DSS (cell line) - DSS (PBMC).
1C: Mean differential robust z-scores of siRNAs to validate hits from screen.
1D: Percent viability of DHL4, Toledo, Riva, and U2932 cells siRNA knockdowns of GAK, PI3Kδ, PTK2B, and a non-targeting (siNT) compared to parental cell lines. Data represent mean ± SEM from four technical replicates. ****$p<0.0001$ compared to si untreated.

1E: Dose response viability assays of DHL4, Toledo, RIVA, and U2932 cells treated with SGC-GAK-1 and SGC-GAK-1N for 72 hours. Data represent mean ± SEM from four technical replicates.

Figure 2: GAK inhibition is broadly active against DLBCL, with increased sensitivity in ABC subtypes, while not impacting B-cell receptor signaling or recycling
2A: GI_{50} values calculated from growth inhibition assays of a panel of GCB and ABC DLBCL cell lines and PBMCs treated with SGC-GAK-1.
2B: Box plot of GI_{50} values comparing GCB and ABC DLBCL cell lines treated with SGC-GAK-1. P = 0.0078 **.
2C: Western blot of proteins implicated in B-cell receptor signaling, including AKT, phosphorylated AKT, ERK, and phosphorylated ERK, in SGC-GAK-1 (1 µM) treated DHL4 cells.
2D: Measurement of IgM-A to measure B-cell surface expression via flow cytometry of RIVA cells treated with DMSO vehicle and SGC-GAK-1 5 µM.

Figure 3: GAK inhibition triggers induction of the mitotic spindle assembly checkpoint and G2/M-phase cell-cycle arrest
3A: Western blot of proteins implicated in cell-cycle arrest, including BubR1, Cyclin B1, Histone H3, and phosphorylated Histone H3, in SGC-GAK-1 (10 µM) treated RIVA, DHL4, Toledo, and U2932 cells for 24 hours.
3B: Cell cycle analysis by flow cytometry of RIVA, U2932, DHL4, and Toledo cells treated with DMSO vehicle, SGC-GAK-1 10 µM, and flavopiridol 500nM for 24 hours.
3C: Confocal immunofluorescent imaging of U2932, RIVA, TMD8, and PBMC cells treated with DMSO vehicle and SGC-GAK-1 1 µM for 24 hours. Chromosomes pictured red and alpha-tubulin green.
3D: Violin plots demonstrate immunofluorescence quantification of DAPI stained chromosomes following 24hr 1µM SGC-GAK-1 treatment of cells compared to DMSO vehicle treatment. Red arrows indicate G1 and G2 cell cycle phases. ****$p<0.0001$, **$p<0.01$.

Figure 4: GAK expression associates with cell cycle activation in DLBCL cases
4A: Reddy and Lenz data show enriched genesets in *GAK*-high vs *GAK*-low cases from FGSEA analyses (adjusted $p<0.05$, log-2 fold change >0.5).
4B: FGSEA Hallmark pathway analysis of upregulated genes in U2932 and Ly1 cells treated with SGC-GAK-1 1 µM for 12 hours compared to DMSO vehicle (adjusted $p<0.05$, log-2 fold change >0.5).
4C: Western blot of proteins implicated in cell-cycle arrest, including Histone H3 and phosphorylated Histone H3, in SGC-GAK-1 (1 µM) and Alisertib (1 µM) treated U2932 cells for 24 hours.
4G: Heatmap of Bliss synergy scores from U2932, RIVA, DHL4, and Ly1 cells treated with SGC-GAK-1 in combination with DLBCL chemotherapeutics and cell cycle inhibitors.

Figure 5: GAK dependence is strongly linked to retinoblastoma loss of function in DLBCL
5A-B: Lenz (A) and Reddy (B) data show low *RB1* associated with increased *GAK*. p=2.13e-22 *RB1* expression difference by *GAK* group (Lenz); p=2.2e-16 (Wilcoxon) Q1 vs Q4 (Reddy).

5C: Western blot of DLBCL cell lines probed for GAK and RB. RIVA and U2932 completely lack RB.
5D: Cell cycle analysis by flow cytometry on U2932, RIVA, and DHL4 cells treated with DMSO vehicle, SGC-GAK-1 1 µM, and GAK-sparing analog 1N 1 µM for 24 hours.
5E: Western blot of U2OS WT, *RB1*+/-, and *RB1*-/- CRISPR-modified cells probed for RB.
5F: Dose response growth inhibition assay of U2OS WT and RB-deficient cells treated with SGC-GAK-1.
5G: Confocal immunofluorescent imaging of U2OS WT and *RB1*-/- cells treated with DMSO vehicle and SGC-GAK-1 1 µM for 24 hours. Chromosomes pictured red and alpha-tubulin green.
5H: Violin plots demonstrate immunofluorescence quantification of DAPI stained chromosomes following 24hr 1µM SGC-GAK-1 treatment of U2OS WT and *RB1*-/- cells compared to DMSO vehicle treatment. ****$p<0.0001$, *$p<0.05$.

Figure 6: Efficacy of GAK inhibition *in vivo*
6A: Average tumor volume ± SEM measured via IVIS of xenograft U2932 cells in NSG mice treated with SGC-GAK-1 + ABT and vehicle. *** $p = 0.0003$ (Two way ANOVA).
6B: IVIS images of xenograft U2932 cells in NSG mice treated with SGC-GAK-1 + ABT and vehicle.
6C: Immunohistochemical staining Ki67 on tumors derived from lung and liver of animals treated with SGC-GAK-1 + ABT and vehicle.
6D: Kaplan-Meier curves showing survival of SGC-GAK-1 + ABT and vehicle treated groups.
6E: Ex vivo IVIS signal of individual organs derived from SGC-GAK-1 + ABT and vehicle groups. * $p<0.05$.

Figure 7: Candidate clinical drugs for GAK repurposing
7A: Affinities (Kd) for GAK and for the intended clinical target of FDA approved compounds that have GAK as an off-target, derived from biochemical assays.
7B: Dose response curve of NanoBRET® Target Engagement (TE) Intracellular Kinase Assay of SGC-GAK-1, SGC-GAK-1N, and FDA approved compounds, demonstrating affinity for GAK following treatment in NanoLuc®-GAK Fusion Vector transfected 293T cells. NanoBRET Kd calculated from curve-fit regression shown below, including four compounds more potent than the tool compound SGC-GAK-1 (highlighted).
7C: Dose response viability assays of U2932, RIVA, and DHL10 cells treated with Milciclib for 72 hours. Data represent mean ± SEM from three technical replicates.
7D: Dose response viability assays of U2932, RIVA, and DHL10 cells treated with OTS167 for 72 hours. Data represent mean ± SEM from three technical replicates.
7E: Western blot of proteins implicated in cell-cycle arrest, including Histone H3 and phosphorylated Histone H3, in SGC-GAK-1 (1 µM), Milciclib (1 µM, 100nM), and OTS167 (100nM, 10nM, 1nM) treated U2932 cells for 24 hours.
7F: Cell cycle analysis by flow cytometry of U2932 cells treated with DMSO vehicle, Milciclib, and OTS167 at concentrations of 1 µM, 100nM, 10nM, and 1nM for 6, 13, and 24 hours.

References:

1. Teras LR, DeSantis CE, Cerhan JR, et al. 2016 US lymphoid malignancy statistics by World Health Organization subtypes. *CA Cancer J Clin*. 2016;66(6):443–459.
2. Crombie JL, Armand P. Diffuse Large B-Cell Lymphoma's New Genomics: The Bridge and the Chasm. *J Clin Oncol*. 2020;38(30):3565–3574.
3. Alizadeh AA, Eisen MB, Davis RE, et al. Distinct types of diffuse large B-cell lymphoma identified by gene expression profiling. *Nature*. 2000;403(6769):503–11.
4. Lenz G, Wright G, Dave SS, et al. Stromal gene signatures in large-B-cell lymphomas. *N Engl J Med*. 2008;359(22):2313–23.
5. Monti S, Savage KJ, Kutok JL, et al. Molecular profiling of diffuse large B-cell lymphoma identifies robust subtypes including one characterized by host inflammatory response. *Blood*. 2005;105(5):1851–61.
6. Chapuy B, Stewart C, Dunford AJ, et al. Molecular subtypes of diffuse large B cell lymphoma are associated with distinct pathogenic mechanisms and outcomes. *Nat Med*. 2018;24(5):679–690.
7. Wright GW, Huang DW, Phelan JD, et al. A Probabilistic Classification Tool for Genetic Subtypes of Diffuse Large B Cell Lymphoma with Therapeutic Implications. *Cancer Cell*. 2020;37(4):551-568 e14.
8. Coiffier B, Lepage E, Briere J, et al. CHOP chemotherapy plus rituximab compared with CHOP alone in elderly patients with diffuse large-B-cell lymphoma. *N Engl J Med*. 2002;346(4):235–42.
9. Feugier P, Van Hoof A, Sebban C, et al. Long-term results of the R-CHOP study in the treatment of elderly patients with diffuse large B-cell lymphoma: a study by the Groupe d'Etude des Lymphomes de l'Adulte. *J Clin Oncol*. 2005;23(18):4117–26.
10. Tilly H, Gomes da Silva M, Vitolo U, et al. Diffuse large B-cell lymphoma (DLBCL): ESMO Clinical Practice Guidelines for diagnosis, treatment and follow-up. *Ann Oncol*. 2015;26 Suppl 5:v116-25.
11. Coiffier B, Sarkozy C. Diffuse large B-cell lymphoma: R-CHOP failure-what to do? *Hematol. Am Soc Hematol Educ Program*. 2016;2016(1):366–378.
12. Sehn LH, Herrera AF, Flowers CR, et al. Polatuzumab Vedotin in Relapsed or Refractory Diffuse Large B-Cell Lymphoma. *J Clin Oncol*. 2020;38(2):155–165.
13. Tilly H, Morschhauser F, Sehn LH, et al. Polatuzumab Vedotin in Previously Untreated Diffuse Large B-Cell Lymphoma. *N Engl J Med*. 2022;386(4):351–363.
14. Pfreundschuh M, Kuhnt E, Trumper L, et al. CHOP-like chemotherapy with or without rituximab in young patients with good-prognosis diffuse large-B-cell lymphoma: 6-year results of an open-label randomised study of the MabThera International Trial (MInT) Group. *Lancet Oncol*. 2011;12(11):1013–22.
15. Sehn LH, Salles G. Diffuse Large B-Cell Lymphoma. *N Engl J Med*. 2021;384(9):842–858.
16. Chavez JC, Locke FL. A Possible Cure for Refractory DLBCL: CARs Are Headed in the Right Direction. *Mol Ther*. 2017;25(10):2241–2243.
17. Sermer D, Brentjens R. CAR T-cell therapy: Full speed ahead. *Hematol Oncol*. 2019;37 Suppl 1:95–100.
18. Poletto S, Novo M, Paruzzo L, Frascione PMM, Vitolo U. Treatment strategies for patients with diffuse large B-cell lymphoma. *Cancer Treat Rev*. 2022;110:102443.

19. Bachy E, Le Gouill S, Di Blasi R, et al. A real-world comparison of tisagenlecleucel and axicabtagene ciloleucel CAR T cells in relapsed or refractory diffuse large B cell lymphoma. *Nat Med*. 2022;28(10):2145–2154.
20. Westin JR, Oluwole OO, Kersten MJ, et al. Survival with Axicabtagene Ciloleucel in Large B-Cell Lymphoma. *N Engl J Med*. 2023;389(2):148–157.
21. Neelapu SS, Chavez JC, Sehgal AR, et al. Three-year follow-up analysis of axicabtagene ciloleucel in relapsed/refractory indolent non-Hodgkin lymphoma (ZUMA-5). *Blood*. 2024;143(6):496–506.
22. Honigberg LA, Smith AM, Sirisawad M, et al. The Bruton tyrosine kinase inhibitor PCI-32765 blocks B-cell activation and is efficacious in models of autoimmune disease and B-cell malignancy. *Proc Natl Acad Sci U A*. 2010;107(29):13075–80.
23. Lucas F, Woyach JA. Inhibiting Bruton's Tyrosine Kinase in CLL and Other B-Cell Malignancies. *Target Oncol*. 2019;14(2):125–138.
24. Sharma S, Rai KR. Chronic lymphocytic leukemia (CLL) treatment: So many choices, such great options. *Cancer*. 2019;125(9):1432–1440.
25. Younes A, Sehn LH, Johnson P, et al. Randomized Phase III Trial of Ibrutinib and Rituximab Plus Cyclophosphamide, Doxorubicin, Vincristine, and Prednisone in Non-Germinal Center B-Cell Diffuse Large B-Cell Lymphoma. *J Clin Oncol*. 2019;37(15):1285–1295.
26. Melani C, Lakhotia R, Pittaluga S, et al. Combination Targeted Therapy in Relapsed Diffuse Large B-Cell Lymphoma. *N Engl J Med*. 2024;390(23):2143–2155.
27. Nagle SJ, Woo K, Schuster SJ, et al. Outcomes of patients with relapsed/refractory diffuse large B-cell lymphoma with progression of lymphoma after autologous stem cell transplantation in the rituximab era. *Am J Hematol*. 2013;88(10):890–4.
28. Camus V, Tilly H. Managing early failures with R-CHOP in patients with diffuse large B-cell lymphoma. *Expert Rev Hematol*. 2017;10(12):1047–1055.
29. Lee DW, Wu X, Eisenberg E, Greene LE. Recruitment dynamics of GAK and auxilin to clathrin-coated pits during endocytosis. *J Cell Sci*. 2006;119(Pt 17):3502–12.
30. Shimizu H, Nagamori I, Yabuta N, Nojima H. GAK, a regulator of clathrin-mediated membrane traffic, also controls centrosome integrity and chromosome congression. *J Cell Sci*. 2009;122(Pt 17):3145–52.
31. He K, Song E, Upadhyayula S, et al. Dynamics of Auxilin 1 and GAK in clathrin-mediated traffic. *J Cell Biol*. 2020;219(3):.
32. Wolf B, Busso C, Gonczy P. Live imaging screen reveals that TYRO3 and GAK ensure accurate spindle positioning in human cells. *Nat Commun*. 2019;10(1):2859.
33. Al-Ali H, Lee DH, Danzi MC, et al. Rational Polypharmacology: Systematically Identifying and Engaging Multiple Drug Targets To Promote Axon Growth. *ACS Chem Biol*. 2015;10(8):1939–51.
34. Gautam P, Jaiswal A, Aittokallio T, Al-Ali H, Wennerberg K. Phenotypic Screening Combined with Machine Learning for Efficient Identification of Breast Cancer-Selective Therapeutic Targets. *Cell Chem Biol*. 2019;26(7):970-979 e4.
35. Yadav B, Pemovska T, Szwajda A, et al. Quantitative scoring of differential drug sensitivity for individually optimized anticancer therapies. *Sci Rep*. 2014;4:5193.
36. Drewry DH, Wells CI, Andrews DM, et al. Progress towards a public chemogenomic set for protein kinases and a call for contributions. *PLOS ONE*. 2017;12(8):e0181585.

37. Patel AK, Broyer RM, Lee CD, et al. Inhibition of GCK-IV kinases dissociates cell death and axon regeneration in CNS neurons. *Proc Natl Acad Sci U A*. 2020;117(52):33597–33607.
38. Wells CI, Al-Ali H, Andrews DM, et al. The Kinase Chemogenomic Set (KCGS): An Open Science Resource for Kinase Vulnerability Identification. *Int J Mol Sci*. 2021;22(2):.
39. Drewry DH, Wells CI, Andrews DM, et al. Progress towards a public chemogenomic set for protein kinases and a call for contributions. *PLoS One*. 2017;12(8):e0181585.
40. Kaestner P, Stolz A, Bastians H. Determinants for the efficiency of anticancer drugs targeting either Aurora-A or Aurora-B kinases in human colon carcinoma cells. *Mol Cancer Ther*. 2009;8(7):2046–56.
41. Goldenson B, Crispino JD. The aurora kinases in cell cycle and leukemia. *Oncogene*. 2015;34(5):537–45.
42. Kelly KR, Friedberg JW, Park SI, et al. Phase I Study of the Investigational Aurora A Kinase Inhibitor Alisertib plus Rituximab or Rituximab/Vincristine in Relapsed/Refractory Aggressive B-cell Lymphoma. *Clin Cancer Res*. 2018;24(24):6150–6159.
43. Banerjee T, Kim MS, Haslam A, Prasad V. Clinical Trials Portfolio and Regulatory History of Idelalisib in Indolent Non-Hodgkin Lymphoma: A Systematic Review and Meta-analysis. *JAMA Intern Med*. 2023;183(5):435–441.
44. Asquith CRM, Berger BT, Wan J, et al. SGC-GAK-1: A Chemical Probe for Cyclin G Associated Kinase (GAK). *J Med Chem*. 2019;62(5):2830–2836.
45. Korolchuk VI, Banting G. CK2 and GAK/auxilin2 are major protein kinases in clathrin-coated vesicles. *Traffic*. 2002;3(6):428–39.
46. Kametaka S, Moriyama K, Burgos PV, et al. Canonical interaction of cyclin G associated kinase with adaptor protein 1 regulates lysosomal enzyme sorting. *Mol Biol Cell*. 2007;18(8):2991–3001.
47. Olszewski MB, Chandris P, Park BC, Eisenberg E, Greene LE. Disruption of clathrin-mediated trafficking causes centrosome overduplication and senescence. *Traffic*. 2014;15(1):60–77.
48. Zhang L, Gjoerup O, Roberts TM. The serine/threonine kinase cyclin G-associated kinase regulates epidermal growth factor receptor signaling. *Proc Natl Acad Sci U A*. 2004;101(28):10296–301.
49. Bekerman E, Neveu G, Shulla A, et al. Anticancer kinase inhibitors impair intracellular viral trafficking and exert broad-spectrum antiviral effects. *J Clin Invest*. 2017;127(4):1338–1352.
50. Davis RE, Ngo VN, Lenz G, et al. Chronic active B-cell-receptor signalling in diffuse large B-cell lymphoma. *Nature*. 2010;463(7277):88–92.
51. Phelan JD, Young RM, Webster DE, et al. A multiprotein supercomplex controlling oncogenic signalling in lymphoma. *Nature*. 2018;560(7718):387–391.
52. Taylor SS, McKeon F. Kinetochore localization of murine Bub1 is required for normal mitotic timing and checkpoint response to spindle damage. *Cell*. 1997;89(5):727–35.
53. Davenport JW, Fernandes ER, Harris LD, Neale GA, Goorha R. The mouse mitotic checkpoint gene bub1b, a novel bub1 family member, is expressed in a cell cycle-dependent manner. *Genomics*. 1999;55(1):113–7.
54. Luo J, Xu X, Hall H, et al. Histone h3 exerts a key function in mitotic checkpoint control. *Mol Cell Biol*. 2010;30(2):537–49.

55. Choi HJ, Fukui M, Zhu BT. Role of cyclin B1/Cdc2 up-regulation in the development of mitotic prometaphase arrest in human breast cancer cells treated with nocodazole. *PLoS One*. 2011;6(8):e24312.
56. Arguello F, Alexander M, Sterry JA, et al. Flavopiridol induces apoptosis of normal lymphoid cells, causes immunosuppression, and has potent antitumor activity In vivo against human leukemia and lymphoma xenografts. *Blood*. 1998;91(7):2482–90.
57. Reddy A, Zhang J, Davis NS, et al. Genetic and Functional Drivers of Diffuse Large B Cell Lymphoma. *Cell*. 2017;171(2):481-494.e15.
58. Korotkevich G, Sukhov V, Budin N, et al. Fast gene set enrichment analysis. 2021;060012. 10.1101/060012.:
59. Pan-cancer analysis of whole genomes. *Nature*. 2020;578, 82–93. 10.1038/s41586-020-1969–6.:
60. Choy L, Norris S, Wu X, et al. Inhibition of Aurora Kinase Induces Endogenous Retroelements to Induce a Type I/III IFN Response via RIG-I. *Cancer Res Commun*. 2024;4(2):540–555.
61. Laplante M, Sabatini DM. mTOR signaling in growth control and disease. *Cell*. 2012;149(2):274–93.
62. Kschonsak YT, Hoffmann I. Activated ezrin controls MISP levels to ensure correct NuMA polarization and spindle orientation. *J Cell Sci*. 2018;131(10):.
63. Oricchio E, Ciriello G, Jiang M, et al. Frequent disruption of the RB pathway in indolent follicular lymphoma suggests a new combination therapy. *J Exp Med*. 2014;211(7):1379–91.
64. Gong X, Du J, Parsons SH, et al. Aurora A Kinase Inhibition Is Synthetic Lethal with Loss of the RB1 Tumor Suppressor Gene. *Cancer Discov*. 2019;9(2):248–263.
65. Oser MG, Fonseca R, Chakraborty AA, et al. Cells Lacking the RB1 Tumor Suppressor Gene Are Hyperdependent on Aurora B Kinase for Survival. *Cancer Discov*. 2019;9(2):230–247.
66. Feng X, Tang M, Dede M, et al. Genome-wide CRISPR screens using isogenic cells reveal vulnerabilities conferred by loss of tumor suppressors. *Sci Adv*. 2022;8(19):eabm6638.
67. Reddy A, Zhang J, Davis NS, et al. Genetic and Functional Drivers of Diffuse Large B Cell Lymphoma. *Cell*. 2017;171(2):481-494 e15.
68. Marshall AE, Roes MV, Passos DT, et al. RB1 Deletion in Retinoblastoma Protein Pathway-Disrupted Cells Results in DNA Damage and Cancer Progression. *Mol Cell Biol*. 2019;39(16):.
69. Asquith CRM, Bennett JM, Su L, et al. Towards the Development of an In vivo Chemical Probe for Cyclin G Associated Kinase (GAK). *Molecules*. 2019;24(22):.
70. Reinecke M, Brear P, Vornholz L, et al. Chemical proteomics reveals the target landscape of 1,000 kinase inhibitors. *Nat Chem Biol*. 2024;20(5):577–585.
71. Klaeger S, Heinzlmeir S, Wilhelm M, et al. The target landscape of clinical kinase drugs. *Science*. 2017;358(6367):.
72. Mahadevan D, Stejskal A, Cooke LS, et al. Aurora A inhibitor (MLN8237) plus vincristine plus rituximab is synthetic lethal and a potential curative therapy in aggressive B-cell non-Hodgkin lymphoma. *Clin Cancer Res*. 2012;18(8):2210–9.

Figure 1

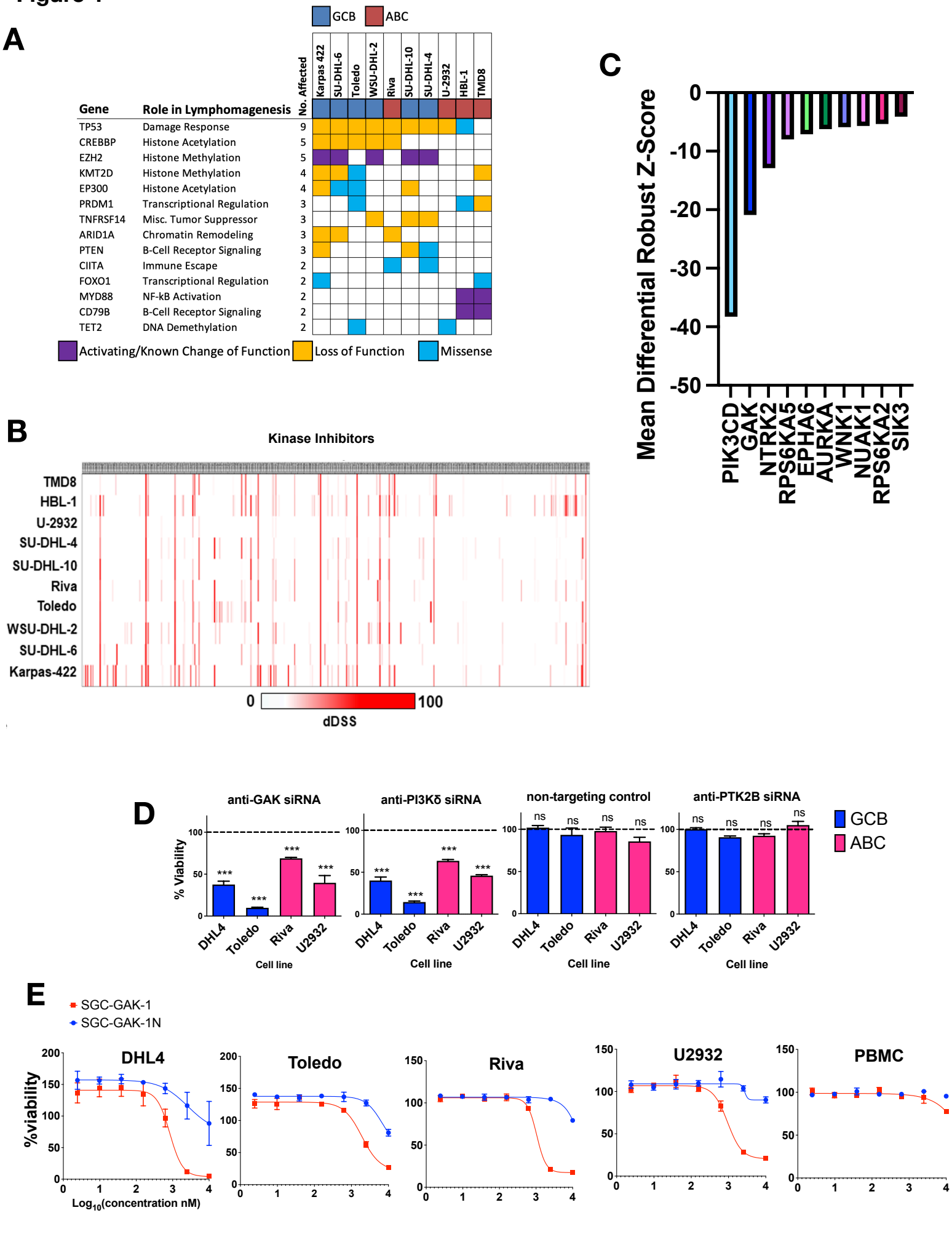
A
GCB
ABC
Karpas 422
SU-DHL-6
Toledo
WSU-DHL-2
Riva
SU-DHL-10
SU-DHL-4
U-2932
HBL-1
TMD8
Gene
Role in Lymphomagenesis
No. Affected
TP53 Damage Response 9
CREBBP Histone Acetylation 5
EZH2 Histone Methylation 5
KMT2D Histone Methylation 4
EP300 Histone Acetylation 4
PRDM1 Transcriptional Regulation 3
TNFRSF14 Misc. Tumor Suppressor 3
ARID1A Chromatin Remodeling 3
PTEN B-Cell Receptor Signaling 3
CIITA Immune Escape 2
FOXO1 Transcriptional Regulation 2
MYD88 NF-kB Activation 2
CD79B B-Cell Receptor Signaling 2
TET2 DNA Demethylation 2
Activating/Known Change of Function
Loss of Function
Missense
C
Mean Differential Robust Z-Score
0
-10
-20
-30
-40
-50
PIK3CD
GAK
NTRK2
RPS6KA5
EPHA6
AURKA
WNK1
NUAK1
RPS6KA2
SIK3
B
Kinase Inhibitors
TMD8
HBL-1
U-2932
SU-DHL-4
SU-DHL-10
Riva
Toledo
WSU-DHL-2
SU-DHL-6
Karpas-422
0
100
dDSS
D
anti-GAK siRNA
anti-PI3Kδ siRNA
non-targeting control
anti-PTK2B siRNA
% Viability
100
50
0
***
ns
DHL4
Toledo
Riva
U2932
Cell line
GCB
ABC
E
SGC-GAK-1
SGC-GAK-1N
DHL4
Toledo
Riva
U2932
PBMC
%viability
200
150
100
50
0
1
2
3
4
Log10(concentration nM)

Figure 2

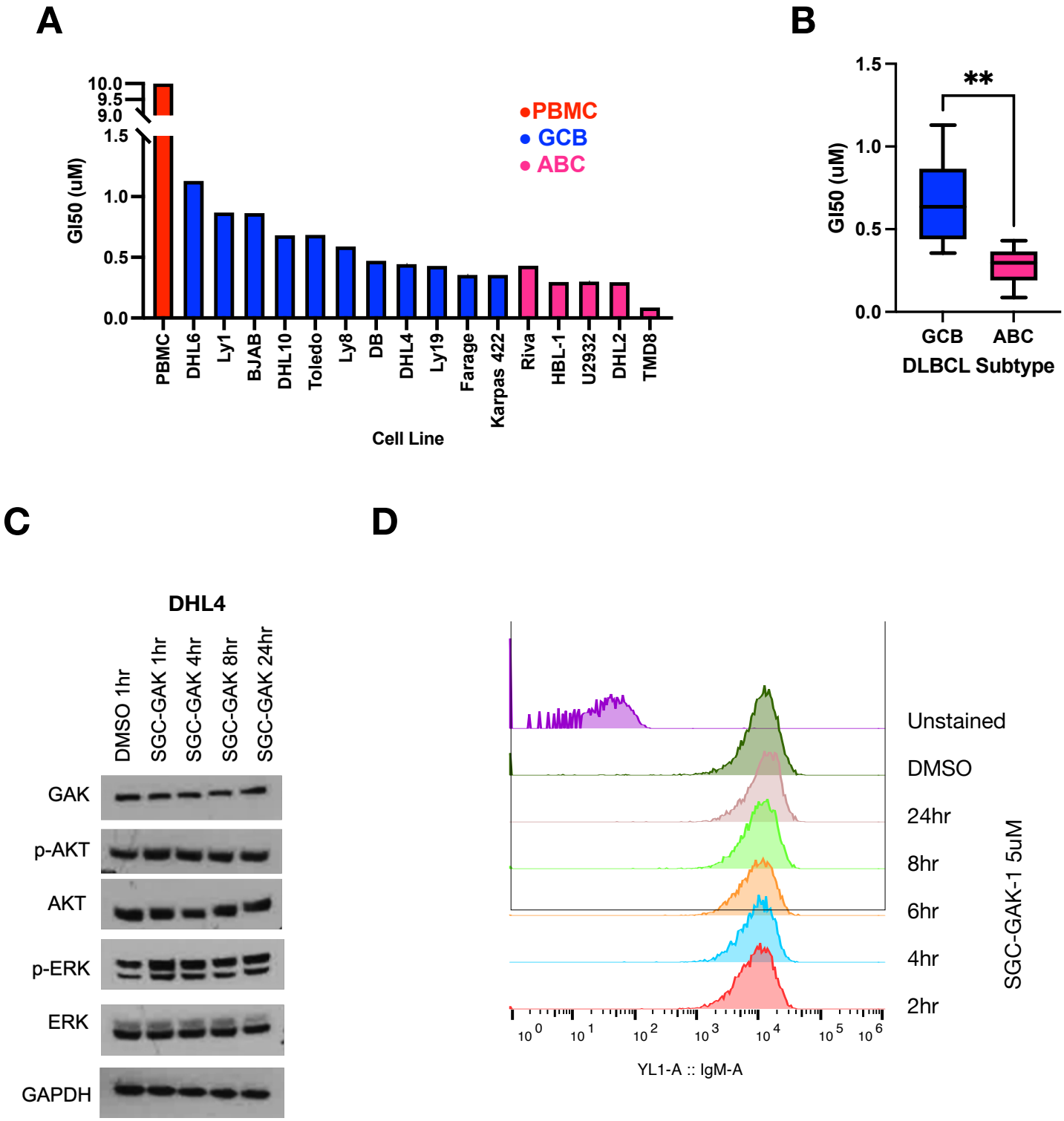
A
GI50 (uM)
10.0
9.5
9.0
1.5
1.0
0.5
0.0
PBMC
GCB
ABC
PBMC
DHL6
Ly1
BJAB
DHL10
Toledo
Ly8
DB
DHL4
Ly19
Farage
Karpas 422
Riva
HBL-1
U2932
DHL2
TMD8
Cell Line
B
GI50 (uM)
1.5
1.0
0.5
0.0
**
GCB
ABC
DLBCL Subtype
C
DHL4
DMSO 1hr
SGC-GAK 1hr
SGC-GAK 4hr
SGC-GAK 8hr
SGC-GAK 24hr
GAK
p-AKT
AKT
p-ERK
ERK
GAPDH
D
Unstained
DMSO
24hr
8hr
6hr
4hr
2hr
SGC-GAK-1 5uM
YL1-A :: IgM-A

Figure 3

A

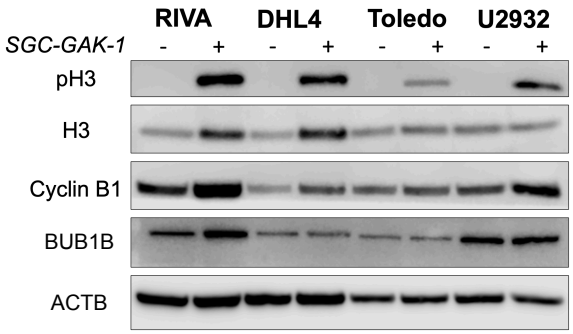

B

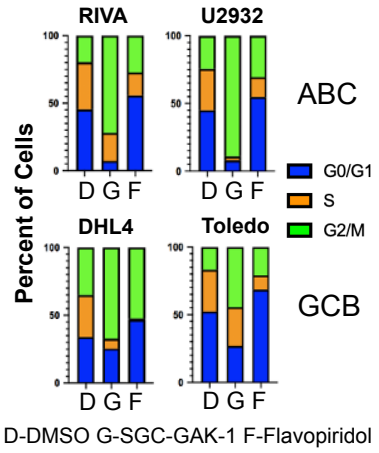

C

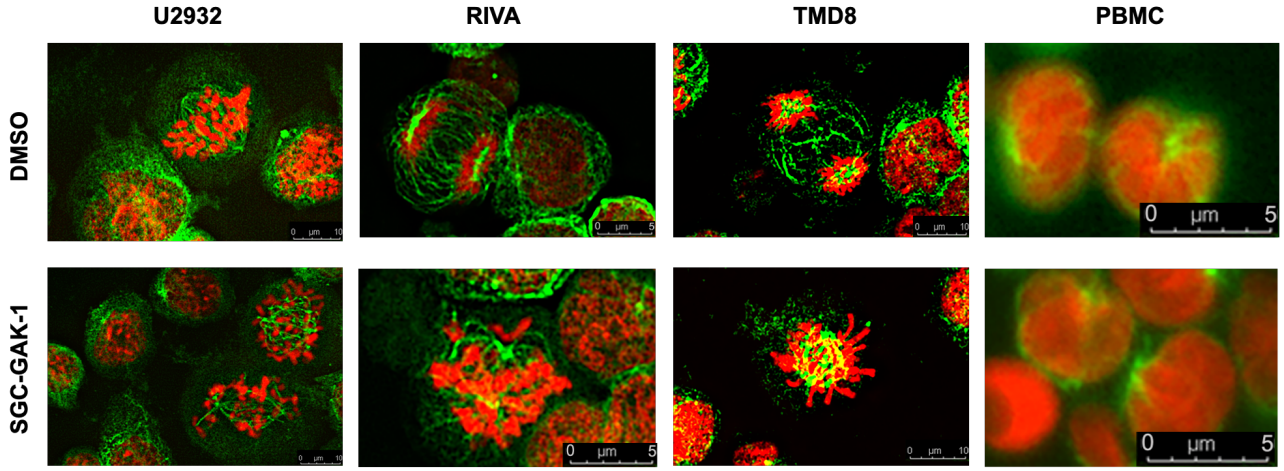

D

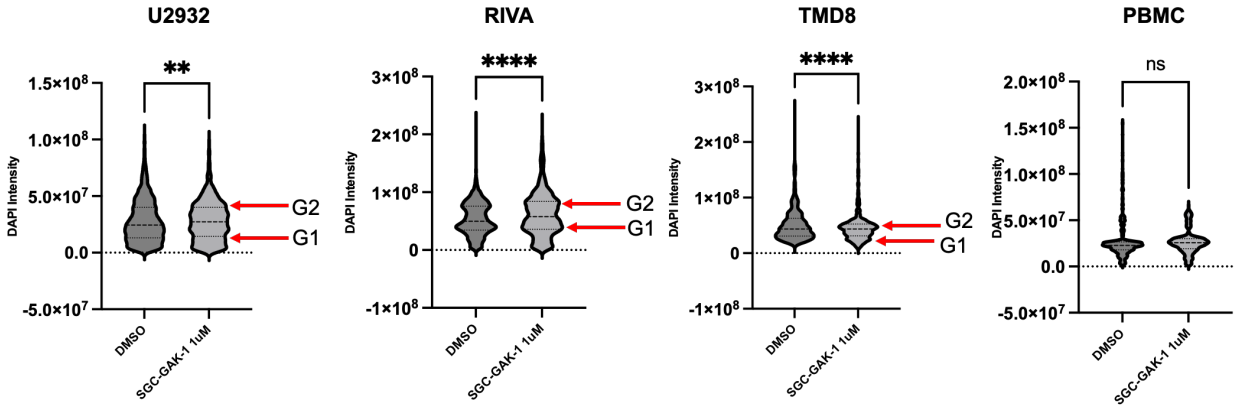

Figure 4

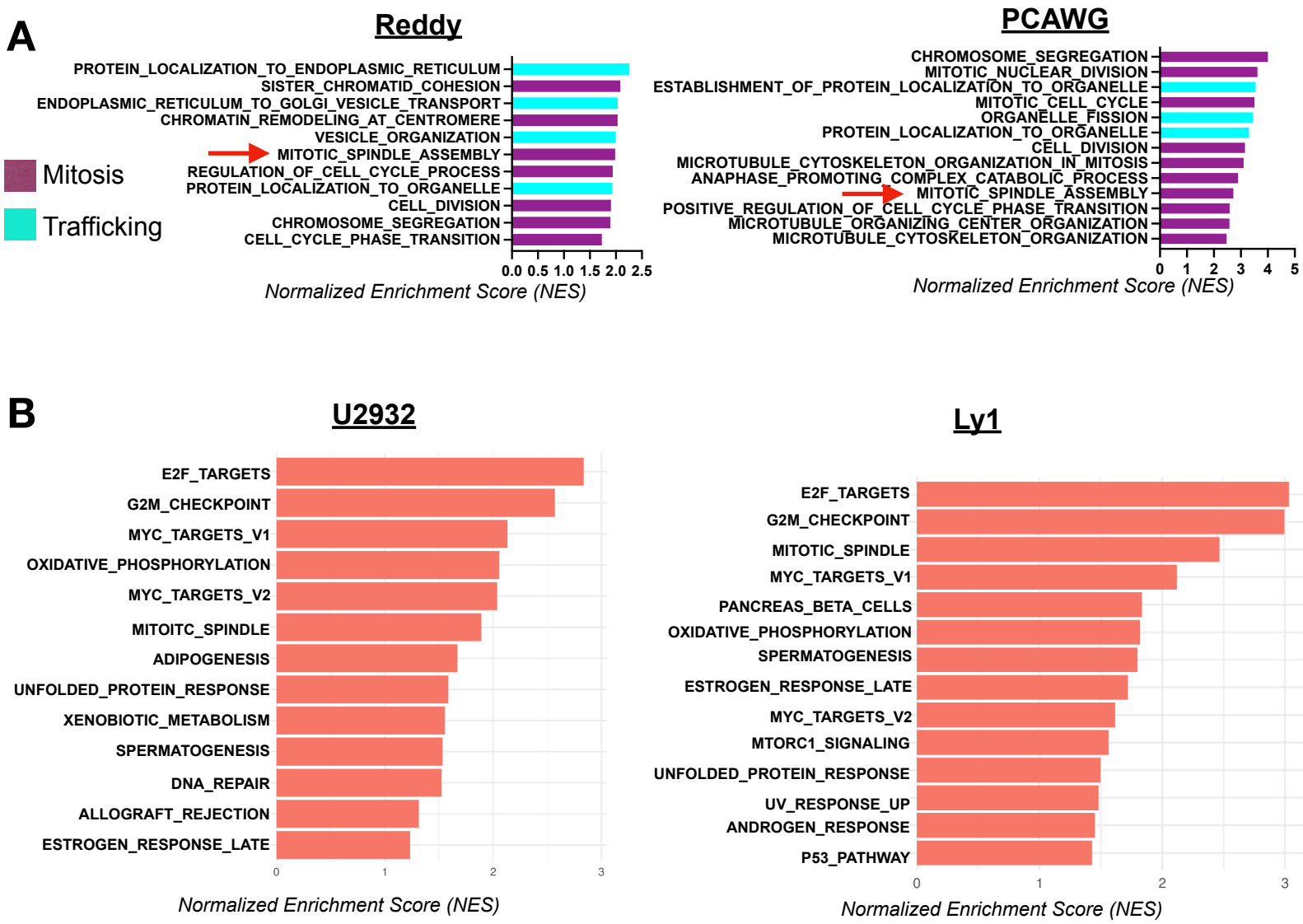
A
Reddy
PROTEIN_LOCALIZATION_TO_ENDOPLASMIC_RETICULUM
SISTER_CHROMATID_COHESION
ENDOPLASMIC_RETICULUM_TO_GOLGI_VESICLE_TRANSPORT
CHROMATIN_REMODELING_AT_CENTROMERE
VESICLE_ORGANIZATION
MITOTIC_SPINDLE_ASSEMBLY
REGULATION_OF_CELL_CYCLE_PROCESS
PROTEIN_LOCALIZATION_TO_ORGANELLE
CELL_DIVISION
CHROMOSOME_SEGREGATION
CELL_CYCLE_PHASE_TRANSITION
0.0 0.5 1.0 1.5 2.0 2.5
Normalized Enrichment Score (NES)
Mitosis
Trafficking
PCAWG
CHROMOSOME_SEGREGATION
MITOTIC_NUCLEAR_DIVISION
ESTABLISHMENT_OF_PROTEIN_LOCALIZATION_TO_ORGANELLE
MITOTIC_CELL_CYCLE
ORGANELLE_FISSION
PROTEIN_LOCALIZATION_TO_ORGANELLE
CELL_DIVISION
MICROTUBULE_CYTOSKELETON_ORGANIZATION_IN_MITOSIS
ANAPHASE_PROMOTING_COMPLEX_CATABOLIC_PROCESS
MITOTIC_SPINDLE_ASSEMBLY
POSITIVE_REGULATION_OF_CELL_CYCLE_PHASE_TRANSITION
MICROTUBULE_ORGANIZING_CENTER_ORGANIZATION
MICROTUBULE_CYTOSKELETON_ORGANIZATION
0 1 2 3 4 5
Normalized Enrichment Score (NES)
B
U2932
E2F_TARGETS
G2M_CHECKPOINT
MYC_TARGETS_V1
OXIDATIVE_PHOSPHORYLATION
MYC_TARGETS_V2
MITOITC_SPINDLE
ADIPOGENESIS
UNFOLDED_PROTEIN_RESPONSE
XENOBIOTIC_METABOLISM
SPERMATOGENESIS
DNA_REPAIR
ALLOGRAFT_REJECTION
ESTROGEN_RESPONSE_LATE
0 1 2 3
Normalized Enrichment Score (NES)
Ly1
E2F_TARGETS
G2M_CHECKPOINT
MITOTIC_SPINDLE
MYC_TARGETS_V1
PANCREAS_BETA_CELLS
OXIDATIVE_PHOSPHORYLATION
SPERMATOGENESIS
ESTROGEN_RESPONSE_LATE
MYC_TARGETS_V2
MTORC1_SIGNALING
UNFOLDED_PROTEIN_RESPONSE
UV_RESPONSE_UP
ANDROGEN_RESPONSE
P53_PATHWAY
0 1 2 3
Normalized Enrichment Score (NES)
C
U2932
pH3
H3
ACTB
DMSO
SGC-GAK-1
Alisertib
D
Synergistic
20
0
-20
Antagonistic
ABC Cell Lines
GCB Cell Lines
U2932
RIVA
DHL4
Ly1
-8.891
-3.787
-8.781
-16.751
-13.144
-30.372
-23.074
-9.586
-11.597
-6.226
-12.351
-10.579
-14.203
-9.284
-15.840
-3.297
-12.270
-8.490
-15.556
-10.028
-16.472
-20.468
-9.932
-20.855
-9.320
-17.009
Doxorubicin
Gemcitabine
Vincristine
Etoposide
Cyclophosphamide
Cisplatin
Bendamustine
Dinaciclib
Nocodazole
Barasertib
Alisertib
Volasertib
Selinexor
DLBCL Chemotherapeutics
Cell Cycle Inhibitors

Figure 5

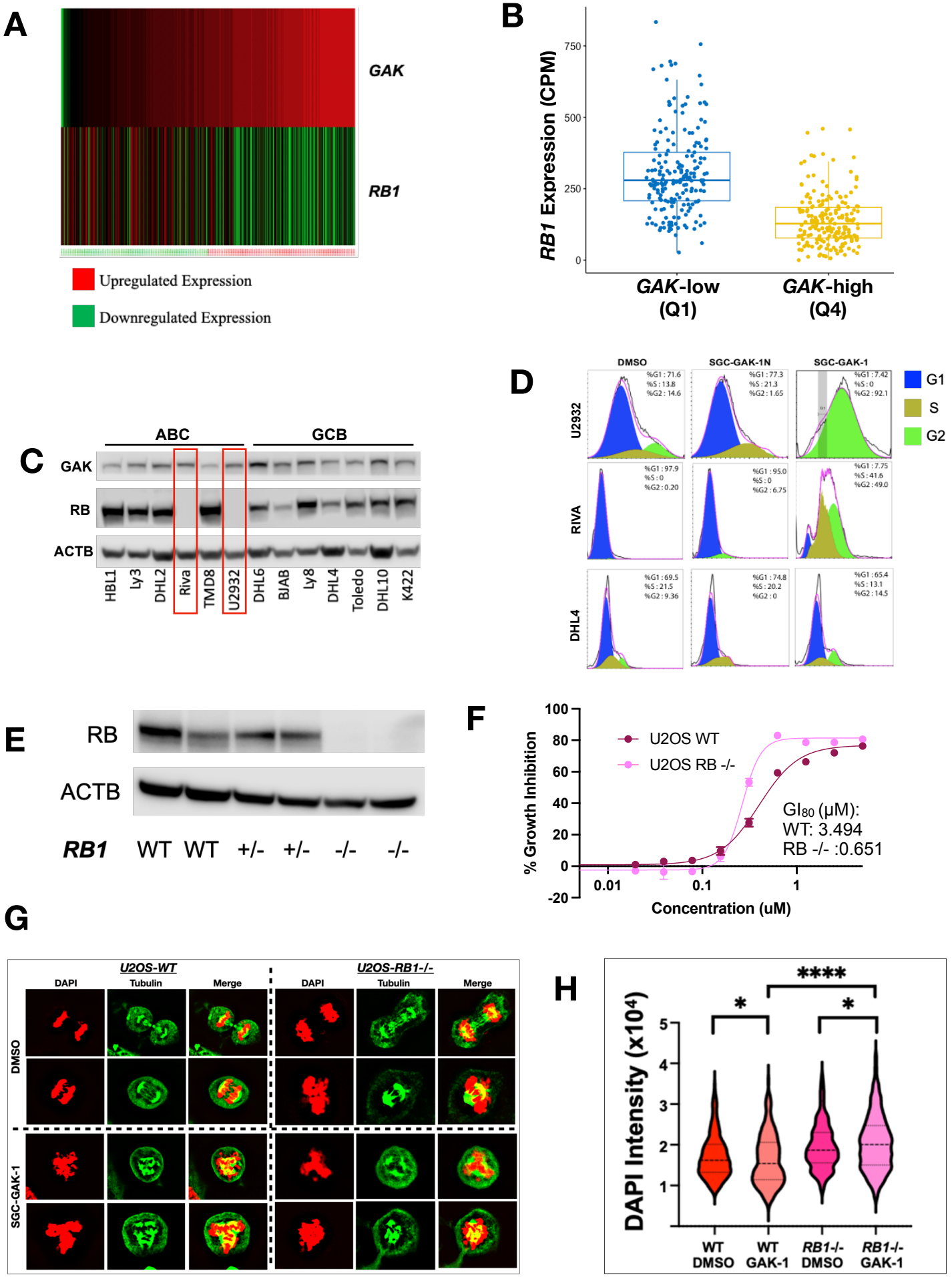
A
GAK
RB1
Upregulated Expression
Downregulated Expression
B
RB1 Expression (CPM)
750
500
250
0
GAK-low (Q1)
GAK-high (Q4)
C
ABC
GCB
GAK
RB
ACTB
HBL1
Ly3
DHL2
Riva
TMD8
U2932
DHL6
BJAB
Ly8
DHL4
Toledo
DHL10
K422
D
DMSO
SGC-GAK-1N
SGC-GAK-1
U2932
RIVA
DHL4
G1
S
G2
E
RB
ACTB
RB1 WT WT +/- +/- -/- -/-
F
% Growth Inhibition
U2OS WT
U2OS RB -/-
GI80 (μM):
WT: 3.494
RB -/- :0.651
Concentration (uM)
G
U2OS-WT
U2OS-RB1-/-
DAPI
Tubulin
Merge
DMSO
SGC-GAK-1
H
DAPI Intensity (x10⁴)
****
*
*
WT DMSO
WT GAK-1
RB1-/- DMSO
RB1-/- GAK-1

Figure 6

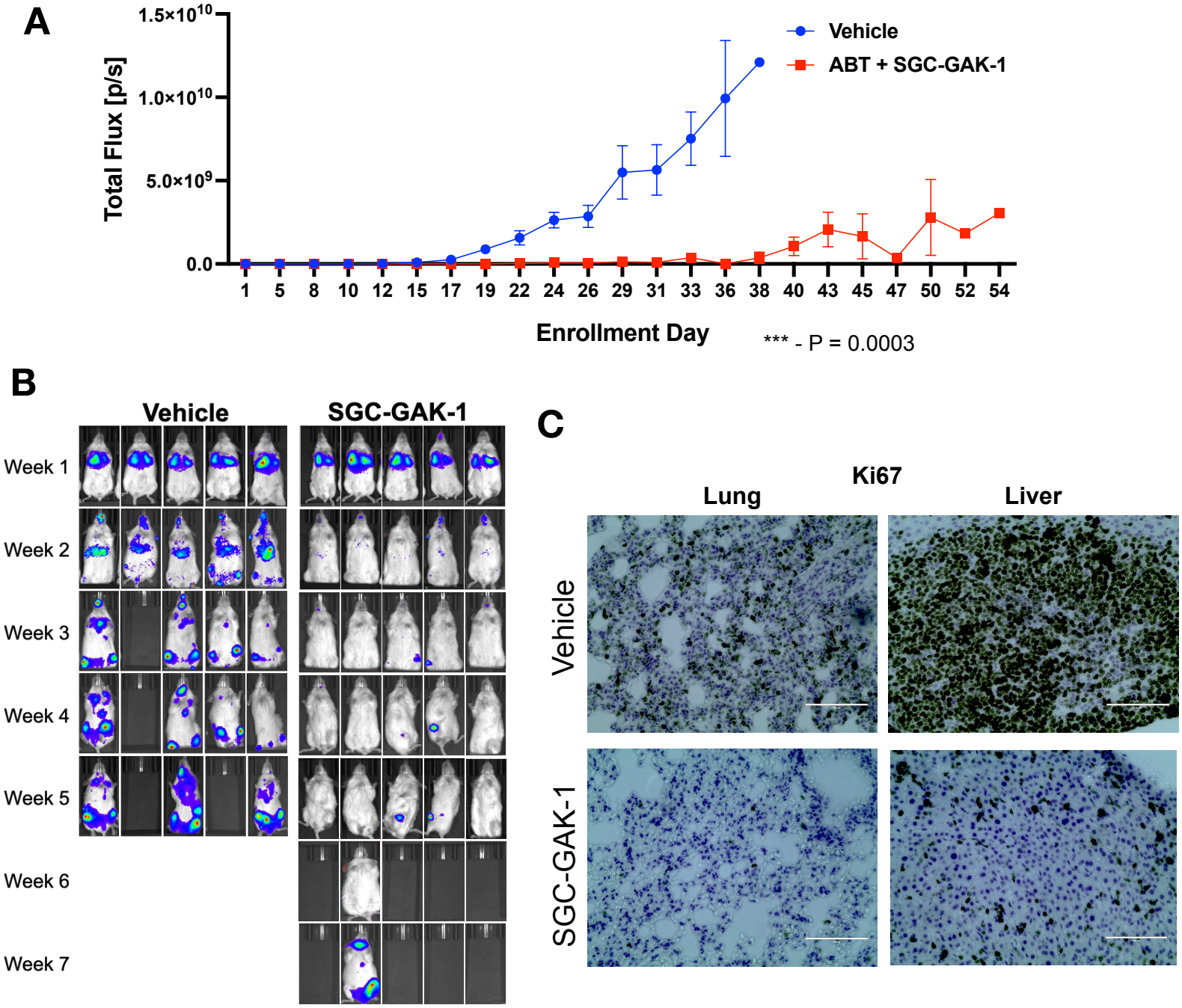
A
Total Flux [p/s]
1.5×10^10
1.0×10^10
5.0×10^9
0.0
Vehicle
ABT + SGC-GAK-1
1 5 8 10 12 15 17 19 22 24 26 29 31 33 36 38 40 43 45 47 50 52 54
Enrollment Day
*** - P = 0.0003
B
Vehicle
SGC-GAK-1
Week 1
Week 2
Week 3
Week 4
Week 5
Week 6
Week 7
C
Ki67
Lung
Liver
Vehicle
SGC-GAK-1

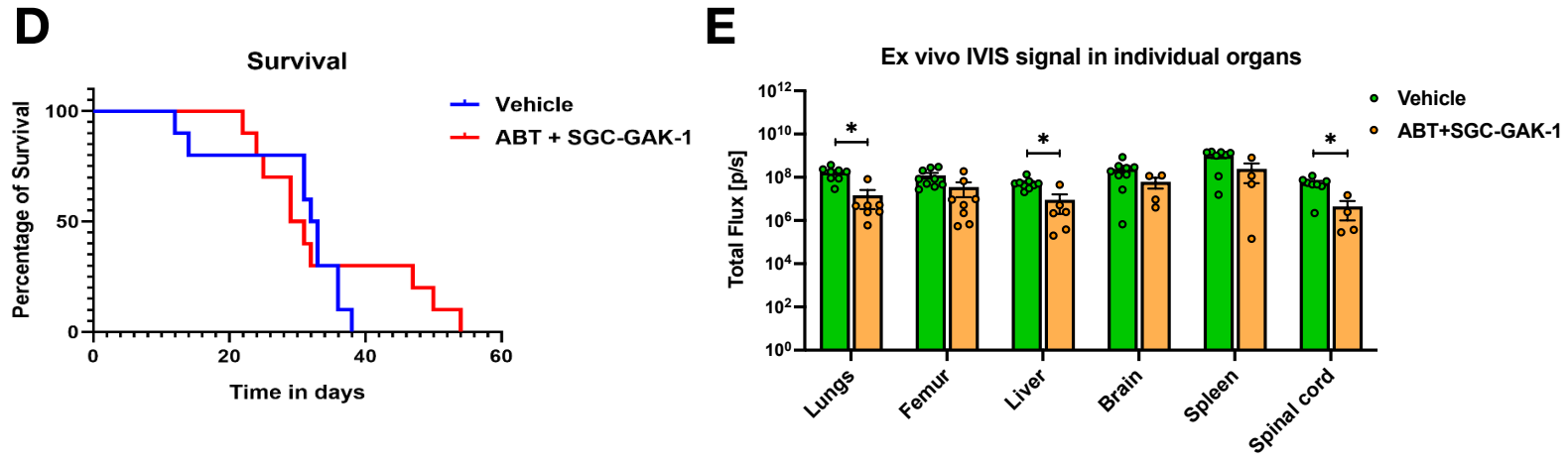
D
Survival
Percentage of Survival
100
50
0
0 20 40 60
Time in days
Vehicle
ABT + SGC-GAK-1
E
Ex vivo IVIS signal in individual organs
Total Flux [p/s]
10^12
10^10
10^8
10^6
10^4
10^2
10^0
Vehicle
ABT+SGC-GAK-1
Lungs
Femur
Liver
Brain
Spleen
Spinal cord

Figure 7

A

Compound	Status	Clinical Targets (Kd)	GAK Kd
Milciclib	Clinical Trials (NSCLC)	CDK7 (285) CDK2 (739)	**3**
OTS167	Clinical Trials (Breast)	MELK (29)	**5**
Gilteritinib	Approved (AML)	FLT3 (7)	**9**
Bosutinib	Approved (CML)	BCR-ABL (3)	**42**
Fedratinib	Approved (MF)	JAK2 (NA)	**46**
Saracatinib	Clinical Trials (pulm fibrosis)	SRC (132)	**108**
Dacomitinib	Approved (NSCLC)	EGFR (5)	**168**
Alectinib	Approved (NSCLC)	ALK (NA)	**259**
Erlotinib	Approved (NSCLC, Pancreatic Ca)	EGFR (2164)	**517**

NSCLC: non-small-cell lung cancer; AML: acute myeloid leukemia; CML: chronic myeloid leukemia; MF: myelofibrosis; NA: not avail.

B

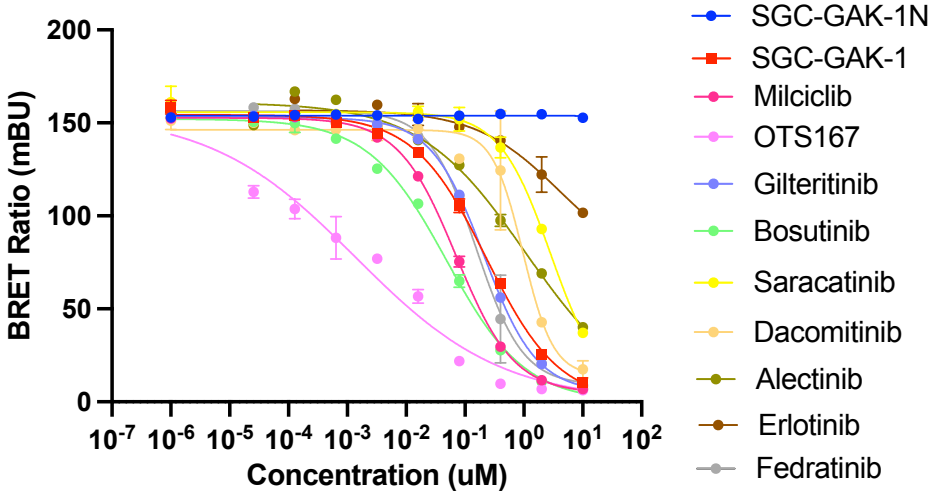

Compound	SGC-GAK-1	SGC-GAK-1N	Milciclib	OTS167	Gilteritinib
NanoBRET Kd (μM)	0.2307	>10	0.07707	0.001394	0.2295
Bosutinib	**Saracatinib**	**Decomitinib**	**Alectinib**	**Erlotinib**	**Fedratnib**
0.04858	3.009	1.159	1.052	>10	0.1804

C

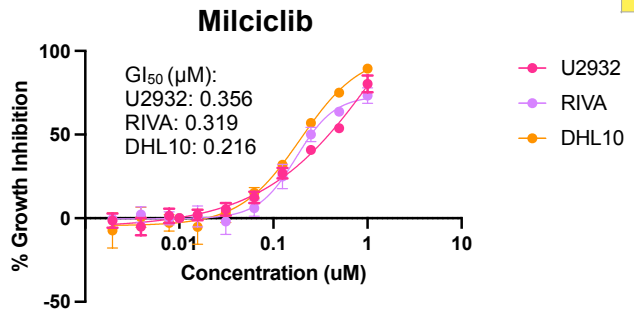

D

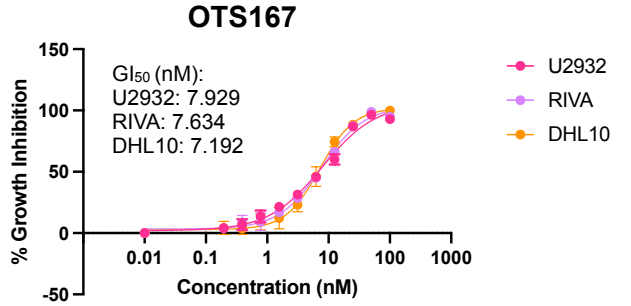

E

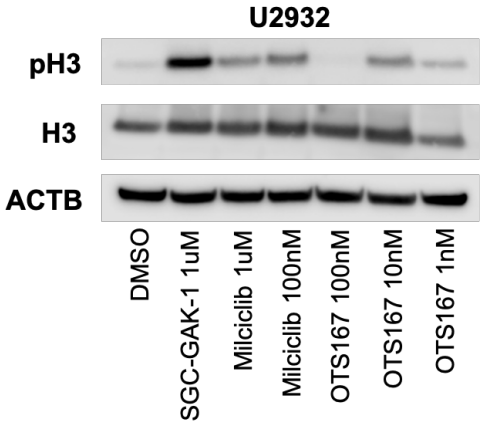
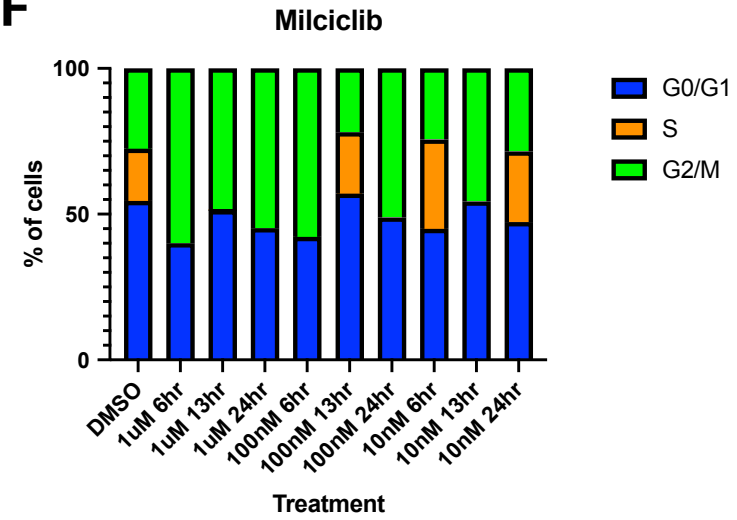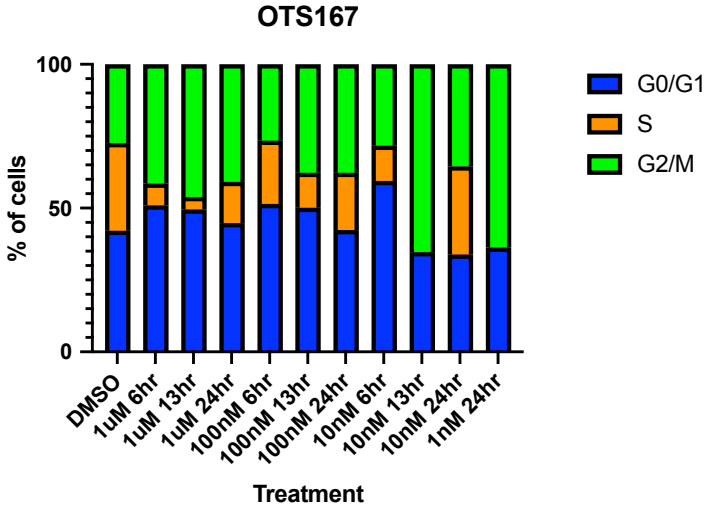
F